Correlated photon-pair generation via single-atom cavity-assisted spontaneous four-wave mixing

Yuan Feng (冯媛), Mao-Hua Wang (王茂桦), Jin-Hui Wu (吴金辉) ⓘ,* and Xiao-Jun Zhang (张晓军) ⓘ†

School of Physics and Center for Quantum Sciences, Northeast Normal University, Changchun 130024, China

We present a detailed study of the generation of photon pairs by spontaneous four-wave mixing in a bicavity system with a single atom inside. Cavity modes lead to larger coupling strength than that of the normally assumed thermal vacuum, and thus higher generation rates are expected. Unlike approaches that have emerged so far, this paper presents an approach based on the solution of the master equation. This method allows us to investigate the photon statistics more strictly, and we show that the choices of pumping detuning and leaking rate of the cavities significantly affect the degree of the autocorrelation, and a higher-purity heralded single photon source is possible. We also derive a concise expression for the output state and the generation rate for the extreme cases where the cavity leaking rate is much smaller or larger than the rate of spontaneous emission.

I. INTRODUCTION

Generating correlated photon pairs (biphotons) is of great interest for developing advanced technologies in quantum information processing [1,2] and it is normally accomplished by the nonlinear parametric processes, such as spontaneous parametric down-conversion (SPDC) [3–5] or spontaneous four-wave mixing (SFWM) [6]. The latter is commonly referred to as the atom-photon interaction with the atomic configuration [7–10] shown in Fig. 1(a). The virtual transition $|1\rangle \rightarrow |4\rangle \rightarrow |2\rangle \rightarrow |3\rangle \rightarrow |1\rangle$ leads to the generation of photons at frequencies ω_s and ω_{as}, which are named the Stokes and anti-Stokes photons, respectively. Apart from the Raman enhancement on the Stokes photon and the absorption on the anti-Stokes photon, there should be a one-to-one correspondence between the two components. The Raman enhancement can be effectively restricted by increasing the detuning of the pumping field [Δ_p in Fig. 1(a)]. As for the absorption of the anti-Stokes photon, the coupling field at ω_c creates a narrow transparency window, which is well known as electromagnetically induced transparency (EIT) [11], and it effectively limits the linewidth of the generated photons.

Narrowband biphotons are particularly important for realizing efficient photon-atom quantum interfaces in a quantum network [12,13], and for better efficiency and greater success rate in quantum memory [14–16] and quantum phase gates [17–19]. From this perspective, the advantage of the biphotons from SFWM is obvious, in contrast to that based on SPDC, which has a relatively large linewidth (~THz) [20,21]. Using optical cavities, a sub-MHz linewidth of the SPDC biphoton can be achieved [22,23]. A similar strategy can be applied to the EIT-assisted SFWM [24], which has not been widely studied yet.

As an important application of the photon pair, heralded single photons [21] promise to enable significant capabil-ities in, e.g., quantum communications [25–27], quantum information [28], quantum metrology [29], and quantum computation [30,31]. In the SFWM process that we focus on, the scheme could be that the detection event of the Stokes photon heralds the presence of the anti-Stokes photon. An ideal single-photon source requires that for a defined mode, the field does not contain more than one photon (high purity). The degree of second-order autocorrelation function, $g^{(2)}_{\text{auto}}(\tau)$, can be a measure of such purity [32,33] and, for the ideal single-photon field, $g^{(2)}_{\text{auto}}(0) = 0$. The high single-photon purity is crucial for the security of quantum communications and minimizing errors in quantum computation and simulation [34–37]. Normally, the SFWM biphoton source is based on the atomic ensembles and, by its nature, low purity is endowed [38].

The recent development of in-cavity quantum electrodynamics, especially that with a single atom [39–42], motivates us to investigate the biphoton source based on a cavity-enhanced single-atom system. As shown in Fig. 1(b), the generation of the photon pairs is triggered by the cavity modes, instead of the thermal vacuum. The bandwidth of the biphoton is determined by the spectral characteristic of the cavities and, in principle, photons with ultralong coherent time can be generated.

The commonly adopted theory for the SFWM is built on the macroscopic nonlinear polarization of atomic ensembles. The brightness and correlations can be described after solving a set of transformed Maxwell equations [43–46], where the third-order (four-wave-mixing) nonlinear susceptibility relates to the coupling between the Stokes and anti-Stokes photons. Or, one can treat the potential energy held by the nonlinear polarization as an effective Hamiltonian, and the corresponding evolution operator acting on the vacuum depicts the state of the output photons [6,47]. Anyway, to obtain the nonlinear susceptibility, we need to presume a preexistent classical field for the Stokes and anti-Stokes photons and solve a (semiclassical) master equation to quantify the nonlinear response of the atoms. Such calculations ought to lead to classical results.
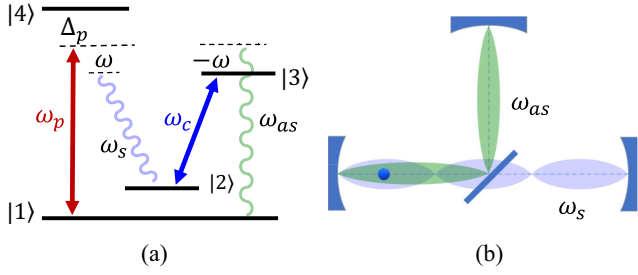
FIG. 1. (a) Four-level atom driven by the pumping field (ω_p) and the coupling field (ω_c) to generate the photon pair (ω_s, ω_{as}). (b) Schematic diagram of the double-cavity system where the size of the atom and the wavelength difference between the Stokes and anti-Stokes photons is dramatically enlarged for better demonstration

The above methods are not suitable for our system where a single atom is coupled by the quantized cavity modes. To obtain the quantum statistics, including the photon distribution, auto- and cross-correlation of generated photons, we resort to the density operator and corresponding (fully quantum) master equation, which is the typical method for describing the interaction between the quantum objects while in contact with non-negligible environments [48,49]. By analyzing the autocorrelation function, we found that the purity of the Stokes or anti-Stokes photon can be controlled by the pumping detuning and the cavity leaking rate, and a high-purity heralded single-photon source is possible without introducing additional nonlinear interaction. Similar to the photon pairs generated by the atomic ensembles, the degree of the cross correlation only acquires considerable values for large pumping detuning. Moreover, by investigating the mean value of atomic operators, we manage to find an effective Hamiltonian for the biphoton generation, and the expression of the biphoton state is derived.

We organize the paper as follows. In Sec. II, we introduce the Hamiltonian and the master equation that depict the dynamic evolution of the system. The brightness and the correlations are discussed in Sec. III. In Sec. IV, we introduce the effective Hamiltonian and the corresponding evolution operator, using which the generation rate is analyzed. We draw our conclusions in Sec. V. The full set of equations of the density matrix elements is listed in the Appendix.

II. MODEL AND EQUATIONS

Let us consider a double-cavity system inside which sits a single four-level ^{87}Rb atom, as shown in Fig. 1. The atomic levels are chosen as $|1\rangle = |5S_{1/2}, F = 1\rangle$, $|2\rangle = |5S_{1/2}, F = 2\rangle$, $|3\rangle = |5P_{1/2}, F = 2\rangle$, and $|4\rangle = |5P_{3/2}, F = 2\rangle$. We further assume that the atomic velocity is small and the Doppler effect can be neglected. Driven by a pumping field at frequency ω_p and a coupling field at ω_c, the atom generates Stokes photons at ω_s and anti-Stokes photons at ω_{as} as cavity modes via the third-order nonlinearity. The Hamiltonian of the interaction is

$$\hat{V}/\hbar = -\Delta_p \hat{\sigma}_{44} + \omega \hat{\sigma}_{22} - \omega \hat{\sigma}_{33}$$
$$- (g_{as}\hat{a}_{as}\hat{\sigma}_{31} + g_s\hat{a}_s\hat{\sigma}_{42} + \Omega_c\hat{\sigma}_{32} + \Omega_p\hat{\sigma}_{41} + \text{H.c.}).$$
$$(1)$$

Here, $\hat{\sigma}_{ij}$ is the atomic operator defined as $|i\rangle\langle j|$. $\Delta_\alpha = \omega_\alpha - \omega_{ij}$ is the detuning of field ω_α with $\alpha \in \{c, p, s, as\}$ from its corresponding transition $|i\rangle \leftrightarrow |j\rangle$. $\omega = \Delta_s - \Delta_p$ is the double-photon detuning between the Stokes photon and pumping field, and, based on the conservation law of energy ($\omega_c + \omega_p = \omega_s + \omega_{as}$), we can write $\Delta_{as} - \Delta_c = -\omega$.

The Rabi frequency of the classical fields ($\Omega_\alpha = \mu_{ij}E_\alpha/2\hbar$) and coupling strength between the cavity modes and the atom ($g_\alpha = \mu_{ij}E_\alpha^+/2\hbar$) are defined in a similar way, where the electric field of a single photon is represented by $\hat{E}_s^+ = \sqrt{(\hbar\omega_s)/(2\epsilon_0 V)}$ and $\hat{E}_{as}^+ = \sqrt{(\hbar\omega_{as})/(2\epsilon_0 V)}$. We assume that the two cavities have the same volume (V). As we can see, the smaller volume leads to larger coupling strength. The confined electric modes play an important role as the environment for the generated photons (instead of vacuum). This ought to increase the efficiency of the photon-pair generation. $\hat{a}_s$ and $\hat{a}_{as}$ are the annihilation operators for the Stokes and anti-Stokes photons, respectively. Using the local approach to the Lindblad superoperators [50–52], the dynamical evolution of the system is governed by the master equation,

$$\frac{\partial}{\partial t}\rho = \frac{i}{\hbar}[\rho, \hat{V}] + \mathscr{L}_{\text{atom}}(\rho) + \mathscr{L}_s(\rho) + \mathscr{L}_{as}(\rho), \quad (2)$$

with $\mathscr{L}_{\text{atom}}(\rho)$, $\mathscr{L}_s(\rho)$, and $\mathscr{L}_{as}(\rho)$ being, respectively, the Lindblad superoperators for the spontaneous decays of the atom, and the Stokes and anti-Stokes photons,

$$\mathscr{L}_{\text{atom}}(\rho) = \Gamma_{31}\left(\hat{\sigma}_{13}\rho\hat{\sigma}_{31} - \tfrac{1}{2}\{\hat{\sigma}_{33}, \rho\}\right)$$
$$+ \Gamma_{32}\left(\hat{\sigma}_{23}\rho\hat{\sigma}_{32} - \tfrac{1}{2}\{\hat{\sigma}_{33}, \rho\}\right)$$
$$+ \Gamma_{41}\left(\hat{\sigma}_{14}\rho\hat{\sigma}_{41} - \tfrac{1}{2}\{\hat{\sigma}_{44}, \rho\}\right)$$
$$+ \Gamma_{42}\left(\hat{\sigma}_{24}\rho\hat{\sigma}_{42} - \tfrac{1}{2}\{\hat{\sigma}_{44}, \rho\}\right); \quad (3a)$$

$$\mathscr{L}_s(\rho) = \kappa_s\left(\hat{a}_s\rho\hat{a}_s^\dagger - \tfrac{1}{2}\hat{a}_s^\dagger\hat{a}_s\rho - \tfrac{1}{2}\rho\hat{a}_s^\dagger\hat{a}_s\right); \quad (3b)$$

$$\mathscr{L}_{as}(\rho) = \kappa_{as}\left(\hat{a}_{as}\rho\hat{a}_{as}^\dagger - \tfrac{1}{2}\hat{a}_{as}^\dagger\hat{a}_{as}\rho - \tfrac{1}{2}\rho\hat{a}_{as}^\dagger\hat{a}_{as}\right). \quad (3c)$$

The decay rate of the atomic transition $|i\rangle \leftrightarrow |j\rangle$ is Γ_{ij}, and κ_s and κ_{as} denote the leaking rates of the photons from corresponding cavity. In the following discussion, we assume that the two cavities have the same leaking rate, and the decay rates of the optical transitions are of the same value as well:

$$\kappa_s = \kappa_{as} = \kappa, \quad (4a)$$

$$\Gamma_{ij} = \Gamma. \quad (4b)$$

We use $\rho_{ij,m_s n_s, m_{as} n_{as}}$ to represent elements of the density matrix $\langle i, m_s, m_{as}|\rho|j, n_s, n_{as}\rangle$, where $|n_s\rangle$ and $|n_{as}\rangle$ are the Fock basis of the Stokes and anti-Stokes photons. Equation (2) leads to a set of differential equations (see the Appendix) taking $\rho_{ij,m_s n_s, m_{as} n_{as}}$ as unknowns. γ_{ij} in those equations represents the dephasing rates due to the interaction with the environment ($\mathscr{L}_{\text{atom}}$), while $\mathscr{D}(\rho_{ij,m_s n_s, m_{as} n_{as}})$ represents dephasing processes owing to the photon leaking from double cavities ($\mathscr{L}_s$ and $\mathscr{L}_{as}$). Additional dephasing processes, e.g., from the finite linewidth of the pumping and coupling field, are omitted since ideal lasers are assumed.

In this paper, we focus on the situation of the steady state where $\partial_t \rho_{ij,m_s n_s, m_{as} n_{as}} = 0$. Thus, the differential equations become algebraic ones. However, finding the exact solutions is still challenging because of the infinite series of the Fock
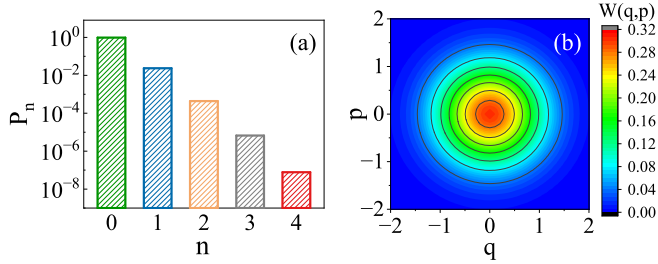
FIG. 2. (a) Stokes photon number probability P_n and (b) the corresponding Wigner functions at large pumping detuning $\Delta_p = 160.0\,\Gamma$. The other parameters are $\kappa = 0.2\,\Gamma$, $\Omega_p = 10.0\,\Gamma$, $\Omega_c = 1.0\,\Gamma$, $\omega = 0$, $\Delta_c = 0$, and $g_a = g_{as} = 1.0\,\Gamma$, $\Gamma = 2\pi \times 6$ MHz. The dipole moment of the optical transition (μ_{ij}) is 2.5×10^{-29} C m and $\omega_{21} = 6.8$ GHz.

states. Considering that the probability of finding one pair of photons should be much larger than that of two pairs, and the probability of two pairs much larger than that of three, we can always choose appropriate parameters, such as the pumping strengths, detunings, and leaking rates, to make the solution reasonable if we truncate the Fock states at a particular one. In the following calculations, we manage to set the boundary at $n_s = n_{as} = 5$.

We first obtain the numerical solution of the master equation when $\kappa = 0.2\,\Gamma$. A smaller leaking rate means a longer lifetime of the cavity photon ($\sim\kappa^{-1}$), and the photon bounces backward and forward between the cavity more times before leaking out. The Stokes photon probability $P_n = \langle n_s | \varrho_s | n_s \rangle$, with ϱ_s being the reduced density matrix for the Stokes field, is presented in Fig. 2(a), with the corresponding Wigner function in Fig. 2(b). Due to the weak interaction between the atom and the cavity modes, the probability of the Stokes field on single-photon state $|1\rangle$, namely, P_1, is about 2.4%, in contrast to P_0, which is close to unity. The Wigner function has positive values, takes (0,0) as the center of symmetry, and resembles that of the ground state of the harmonic oscillator. For the parameters we chose, the anti-Stokes photon has the same quantum statistics as its Stokes partner.

III. BRIGHTNESS AND CORRELATIONS

The SFWM process is not the only nonlinear process supported by the atom; others include the third-order (even fifth-order) Kerr effect, Raman process of the Stokes photon, and the linear and nonlinear absorptions on the anti-Stokes photons. For the inappropriate parameters, the SFWM process might even not be the dominant one.

Presume that SFWM dominates the interaction between the atom and photons; then larger P_1 means that there is a higher probability that the cavity modes are on the biphoton state. There is another quantity similar to the photon probability, which is the (spectral) brightness—the number of photon pairs per unit angular frequency, and time [10,53]. For example, the brightness of the Stokes photon can be represented by the trace of $\rho \hat{a}_s^\dagger \hat{a}_s$. In Fig. 3(a), we plot the brightness of the Stokes and anti-Stokes photons at $\kappa = 0.2\,\Gamma$, for different pumping detunings. As Δ_p increases from zero, the brightness, for both the Stokes and anti-Stokes photons, begins
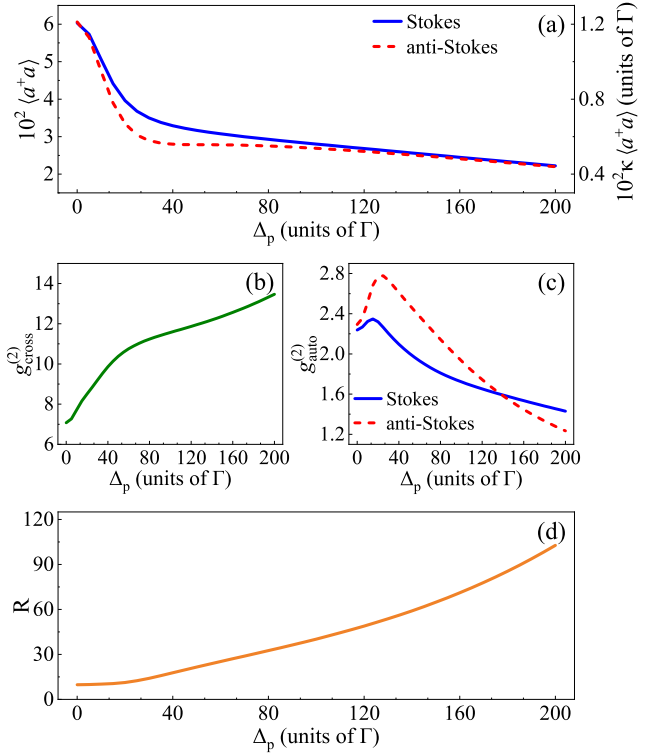

FIG. 3. (a) Spectral brightness, (b) cross correlation, (c) autocorrelation, and (d) the ratio $R = (g_{as,s}^{(2)})^2 / (g_{s,s}^{(2)} g_{as,as}^{(2)})$ of the cavity-enhanced biphoton generation. We use the same parameters as in Fig. 2 with the cavity leaking rate $\kappa = 0.2\,\Gamma$.

to decrease. This is a typical result that the larger pumping detuning weakens the interaction. In addition, the brightness of the Stokes photon is larger than that of the anti-Stokes photon. This is basically due to the fact that the Stokes photons experience Raman enhancement during propagation. As Δ_p gets larger ($\Delta_p > 150\Gamma$), the SFWM becomes the dominant effect and the brightness of the two components takes approximately the same value. As another important figure of merit, the generation rate can be interpreted as the number of photon pairs observed per unit of time. For example, the generation rate of the Stokes photons can be obtained via $R_s = \text{tr}[\rho \mathscr{L}_s(\rho)] = \kappa \langle \hat{a}_s^\dagger \hat{a}_s \rangle$. The left axis of Fig. 3(a) shows the corresponding generation rate, as we can see, for $\Delta_p = 200\,\gamma$, $R_s = 150$ kHz (for $\Gamma = 2\pi \times 6$ MHz), which is much larger than the dark-count rate of the commonly used detectors [53–55].

The one-to-one relation between the Stoke and anti-Stokes photons is essential in the biphoton preparation. The degree of cross-correlation function $g_{\text{cross}}^{(2)}$, defined as $\langle \hat{a}_{as}^\dagger \hat{a}_s^\dagger \hat{a}_s \hat{a}_{as} \rangle / \langle \hat{a}_{as}^\dagger \hat{a}_{as} \rangle \langle \hat{a}_s^\dagger \hat{a}_s \rangle$, is shown in Fig. 3(b); as we can see, when the Stokes and anti-Stokes photons acquire the same brightness, their cross correlation effectively increases as well.

The autocorrelation reveals the nature of the light. Taking the Stokes photons as an example, the degree of the auto-correlation function is $g_{\text{auto}} = \langle \hat{a}_s^\dagger \hat{a}_s^\dagger \hat{a}_s \hat{a}_s \rangle / \langle \hat{a}_s^\dagger \hat{a}_s \rangle \langle \hat{a}_s^\dagger \hat{a}_s \rangle$, which can be measured in a Hanbury Brown and Twiss experiment [56]. Using the number operator $\hat{n}_s = \hat{a}_s^\dagger \hat{a}_s$, it can be rewritten as $g_{\text{auto}} = \langle \hat{n}(\hat{n} - 1) \rangle / \langle \hat{n} \rangle^2$. Thus, for the single-photon field,
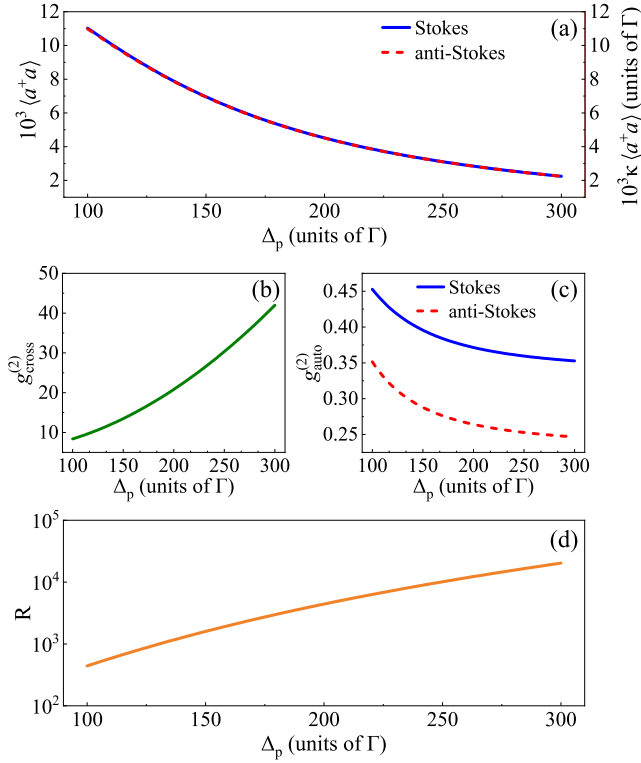
FIG. 4. (a) Spectral brightness, (b) cross correlation, (c) autocorrelation, and (d) the ratio R under large pumping detuning. Here, $\kappa = 1.0\,\Gamma$ and the other parameters are identical with that in Fig. 2.

$g_{\text{auto}} = 0$. The data we presented in Fig. 3(c) show that the degree of autocorrelation is above zero, indicating that there are multiple photons in the Stokes field, and likewise for the anti-Stokes partner. They begin to decrease when pumping detuning is larger than $30\,\Gamma$ and keep decreasing as Δ increases. However, they are still above unity for Δ_p as large as $200\,\Gamma$.

The violation of $(g_{as,s}^{(2)})^2/(g_{s,s}^{(2)}g_{as,as}^{(2)}) \leqslant 1$, widely known as Cauchy-Schwarz inequality, is commonly regarded as an unambiguous feature of the nonclassical correlation between the generated photons [57]. The quantity

$$R = \frac{\left(g_{as,s}^{(2)}\right)^2}{g_{s,s}^{(2)}g_{as,as}^{(2)}}$$

is plotted in Fig. 3(d). It has an initial value of $R \approx 9.8$ and increases almost linearly with the pumping detuning.

Enlarging the decay rate of the cavities naturally reduces the energy stored in the cavity. As can be seen in Fig. 4(a), the brightness of, e.g., the Stokes photon for $\kappa = 1.0\,\Gamma$ is almost 10 times smaller than that for $\kappa = 0.2\,\Gamma$. At the price of this, the brightness of the Stokes and anti-Stokes photons takes almost the same value, suggesting that the efficiency of the Raman effect on the Stokes photon is effectively reduced for larger κ, and the degree of the cross correlation, as shown in Fig. 4(b), is correspondingly enhanced. The result of the cross correlation and the autocorrelation leads to a surprising result that the Cauchy-Schwarz inequality could be violated by a factor over 10^4 at $\Delta = 300\,\Gamma$ with a generation rate of approximately 75 kHz, according to our idealized theoretical calculation.

IV. EFFECTIVE HAMILTONIAN AND GENERATION RATES

The numerical results show the characteristics of the system in a straightforward manner, such as the data presented in Figs. 2 and 3. As long as the Fock states are reasonably truncated, the solution of the master equation, equivalently the plotted data, to some extent, is exact. However, these results are not transparent for revealing the underlying physics of the atom-photon interaction. The analytic solutions may provide us with useful information, but it is difficult to obtain.

Fortunately, as we discussed in Sec. III, a large cross correlation relies on the large pumping detunings, and this means that the atom most likely remains on the ground level $|1\rangle$, which allows us to make a series of assumptions to find an effective Hamiltonian and evolution operators. First, let us examine the motion equations for the atomic operators in the Heisenberg picture,

$$\partial_t \hat{\sigma}_{44} = -(\Gamma_{41} + \Gamma_{42})\hat{\sigma}_{44} + [i(g_s\hat{a}_s\hat{\sigma}_{42} + \Omega_p\hat{\sigma}_{41}) + \text{H.c.}],$$

$$\partial_t \hat{\sigma}_{33} = -(\Gamma_{31} + \Gamma_{32})\hat{\sigma}_{33} + [i(g_{as}\hat{a}_{as}\hat{\sigma}_{31} + \Omega_c\hat{\sigma}_{32}) + \text{H.c.}],$$

$$\partial_t \hat{\sigma}_{22} = \Gamma_{32}\hat{\sigma}_{33} + \Gamma_{42}\hat{\sigma}_{44} + [i(g_s\hat{a}_s^\dagger\hat{\sigma}_{24} + \Omega_c^*\hat{\sigma}_{23}) + \text{H.c.}],$$

$$\partial_t \hat{\sigma}_{34} = i(\widetilde{\gamma}_{34}\hat{\sigma}_{34} - g_{as}\hat{a}_{as}^\dagger\hat{\sigma}_{14} - \Omega_c^*\hat{\sigma}_{24} + g_s\hat{a}_s\hat{\sigma}_{32} + \Omega_p\hat{\sigma}_{31}),$$

$$\partial_t \hat{\sigma}_{24} = i[\widetilde{\gamma}_{24}\hat{\sigma}_{24} + g_s\hat{a}_s(\hat{\sigma}_{22} - \hat{\sigma}_{44}) - \Omega_c\hat{\sigma}_{34} + \Omega_p\hat{\sigma}_{21}],$$

$$\partial_t \hat{\sigma}_{14} = i[\widetilde{\gamma}_{14}\hat{\sigma}_{14} - g_{as}\hat{a}_{as}\hat{\sigma}_{34} + \Omega_p(\hat{\sigma}_{11} - \hat{\sigma}_{44}) + g_s\hat{a}_s\hat{\sigma}_{12}],$$

$$\partial_t \hat{\sigma}_{23} = i[\widetilde{\gamma}_{23}\hat{\sigma}_{23} - g_s\hat{a}_s\hat{\sigma}_{43} + \Omega_c(\hat{\sigma}_{22} - \hat{\sigma}_{33}) + g_{as}\hat{a}_{as}\hat{\sigma}_{21}],$$

$$\partial_t \hat{\sigma}_{13} = i[\widetilde{\gamma}_{13}\hat{\sigma}_{13} + g_{as}\hat{a}_{as}(\hat{\sigma}_{11} - \hat{\sigma}_{33}) - \Omega_p\hat{\sigma}_{43} + \Omega_c\hat{\sigma}_{12}],$$

$$\partial_t \hat{\sigma}_{12} = i(\widetilde{\gamma}_{12}\hat{\sigma}_{12} - g_{as}\hat{a}_{as}\hat{\sigma}_{32} - \Omega_p\hat{\sigma}_{42} + g_s\hat{a}_s^\dagger\hat{\sigma}_{14} + \Omega_c^*\hat{\sigma}_{13}).$$

In the above equations, we omit fluctuation terms, as we only focus on the mean values in the following calculation. The complex decay rates are defined as $\widetilde{\gamma}_{34} = (\Delta_p - \omega) + i\gamma_{43}$, $\widetilde{\gamma}_{24} = \Delta_p + \omega + i\gamma_{42}$, $\widetilde{\gamma}_{14} = \Delta_p + i\gamma_{41}$, $\widetilde{\gamma}_{23} = 2\omega + i\gamma_{32}$, $\widetilde{\gamma}_{12} = -\omega$, and $\widetilde{\gamma}_{31} = -\omega + i\gamma_{31}$.

Under the assumption of $\Delta_p \gg \Gamma$, we can treat $\hat{\sigma}_{11} = \hat{\mathbb{1}}$, where $\hat{\mathbb{1}}$ is the unit operator, and the other population operator $\hat{\sigma}_{22}$, $\hat{\sigma}_{33}$, and $\hat{\sigma}_{44}$ as zeros. The transition operator $\hat{\sigma}_{41}$ is non-negligible due to the fact that the optical response of the atoms at the frequency ω_p relates to the population on ground level $|1\rangle$. The natural broadening of the transition $|4\rangle \leftrightarrow |1\rangle$ suggests a typical Lorentz line shape as $\hat{\sigma}_{41} = \hat{\sigma}_{14}^\dagger = \alpha_{41}\hat{\mathbb{1}}$, with $\alpha_{14} = \alpha_{41}^* = -\Omega_p/(\Delta_p + i\gamma_{41})$. On the other hand, the optical response at frequency ω_c is negligible ($\hat{\sigma}_{32} = 0$) since the relevant atomic levels are empty.

The Stokes (anti-Stokes) photons are generated through the polarization of $|4\rangle \leftrightarrow |2\rangle$ ($|3\rangle \leftrightarrow |1\rangle$). The relevant atomic operators, based on the motion equations, are coupled with each other as

$$\frac{\partial}{\partial t}\begin{pmatrix}\hat{\sigma}_{34} \\ \hat{\sigma}_{24} \\ \hat{\sigma}_{31} \\ \hat{\sigma}_{21}\end{pmatrix} = i\begin{pmatrix}\widetilde{\gamma}_{34} & -\Omega_c^* & \Omega_p & 0 \\ -\Omega_c & \widetilde{\gamma}_{24} & 0 & \Omega_p \\ \Omega_p^* & 0 & \widetilde{\gamma}_{31} & -\Omega_c^* \\ 0 & \Omega_p^* & -\Omega_c & \omega\end{pmatrix}\begin{pmatrix}\hat{\sigma}_{34} \\ \hat{\sigma}_{24} \\ \hat{\sigma}_{31} \\ \hat{\sigma}_{21}\end{pmatrix}$$
$$+ i(\alpha_{14}g_{as}\hat{a}_{as}^\dagger, 0, g_{as}\hat{a}_{as}^\dagger, \alpha_{41}g_s\hat{a}_s)^{\text{T}}, \quad (5)$$

where $(\cdot)^{\mathrm{T}}$ stands for the transpose of the vector. As the pumping detuning gets larger, all atomic operators in Eq. (5) tend to zero, except for $\hat{\sigma}_{31}$, which can be written as $\hat{\sigma}_{31} = \alpha_{31}\hat{a}_s$, with

$$\alpha_{31} = \frac{\Omega_c^* \Omega_p^* g_s}{[|\Omega_c|^2 + \omega(\omega - i\gamma_{31})](\Delta_p - i\gamma_{41})}. \tag{6}$$

Then we can rewrite Eq. (1) based on the above conclusions, and find that the effective Hamiltonian is

$$\hat{V}_{\mathrm{eff}} = \hbar\alpha_{31}g_{as}\hat{a}_s\hat{a}_{as} + \hbar\alpha_{13}g_{as}\hat{a}_s^\dagger\hat{a}_{as}^\dagger, \tag{7}$$

where α_{13} is the complex conjugate of α_{31}. The corresponding evolution operator in Schrodinger representation on the first order of perturbation [49] is

$$\hat{U}(t_i, t_f) = \hat{\mathbb{1}} - \frac{i}{\hbar}\int_{t_i}^{t_f} dt\, \hat{V}_{\mathrm{eff}}\, e^{-i(\omega_p + \omega_c - \omega_s - \omega_{as})t}. \tag{8}$$

The biphoton state can be represented by the evolution operator acting on the vacuum. After omitting the trivial operator $\hat{\mathbb{1}}$, the output state reads

$$\Psi_{\mathrm{out}} = \hat{U}(t_i, t_f)|0_s, 0_{as}\rangle = \beta|1_s, 1_{as}\rangle. \tag{9}$$

Note that β, whose magnitude represents the strength of the four-wave-mixing process, plays a similar role as the nonlinear susceptibility in the atomic-ensemble situation. The conservation of energy ($\omega_p + \omega_c - \omega_s - \omega_{as} = 0$) is always fulfilled; therefore, $\hat{U}$ and β are determined by the time of evolution $\Delta t = t_f - t_i$ [see Eq. (8)]. Ideally, t_i can be the time when the applied lasers are switched on, and t_f is the time of turning off. This is only reasonable when the evolution is unitary [49]. In our case, the condition means negligible Lindblad superoperators [Eqs. 3(a)–(3c)]. However, interactions between the main system and the unobserved ones [48] always exist in our model, and leaking photons are even necessary for the biphoton generation. All in all, the evolution time is determined by the finite coherent time, which, in turn, relies on the strengths of the damping processes (Γ and κ). However, the detailed relation could be complex. In the following, we only discuss two extreme cases:

(i) $\kappa \gg \Gamma$. In this case, the generated photons escape and quickly impinge on the detector. The coherence time depends on the reciprocal of κ; consequently, β denoted as β_1 in this case, based on Eq. (8), is

$$\beta_1 = -i\alpha_{13}g_{as}/\kappa. \tag{10a}$$

(ii) $\kappa \ll \Gamma$. This means that the generated photons have a relatively long lifetime in their cavity. It is the vacuum as a reservoir coupling directly with the atom that shortens the coherence time; thus β in this case takes the value of

$$\beta_2 = -i\alpha_{13}g_{as}/\Gamma. \tag{10b}$$

Let us apply Eqs. (10a) and (10b) to analyze the generation rate of the photon pair. In Fig. 5, it is plotted using the dark-blue solid line as a function of the leaking rate. For a vanishing κ, the generated photons are trapped inside the cavity, and thus the generated rate tends to zero. The result in case (i) based on Eqs. (10a) and (9) is $R_s = \kappa\langle\Psi_{\mathrm{out}}|\hat{a}_s^\dagger\hat{a}_s|\Psi_{\mathrm{out}}\rangle = |\alpha_{13}g_{as}/\Gamma|^2\kappa$, increasing linearly with κ as shown by the green dashed line. As we can see, it matches the numerical result quite
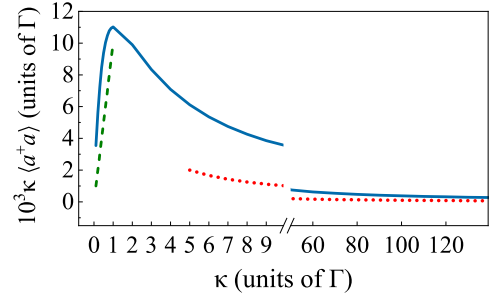

FIG. 5. The results of the generation rate obtained using the method of the effective Hamiltonian, under the assumption of $\kappa \ll \Gamma$ (dashed line) and $\kappa \gg \Gamma$ (dotted line). For ease of comparison, the result of $\mathrm{tr}[\rho\mathscr{L}_s(\rho)]$ based on the numerical solution of the master equation (solid line) is presented as well. Here, $\Delta_p = 100.0\,\Gamma$ and the other parameters are identical to that in Fig. 2.

well. In case (ii), the generation rate is $R_s = |\alpha_{13}g_{as}|^2/\kappa$. It corresponds to the limit of the bad cavity. In such case, the confinement of the electric field is hampered, the strength of the reduced atom-photon interaction is reduced, and so is the generation rate.

Based on Eq. (9), one can calculate the auto- and cross correlations, and find that

$$g_{\mathrm{cross}}^{(2)} = \frac{1}{|\beta|^2}, \quad g_{s,s}^{(2)} = g_{as,as}^{(2)} = 0. \tag{11}$$

Since $\Delta_p \to \infty$, we have $\beta \to 0$. It explains the tendency of the cross- and autocorrelations at larger pumping detunings, as shown in Fig. 4.

V. SUMMARY

In this paper, we investigate the SFWM process supported by a single atom in the double-cavity system. The generated photons are induced by the optical modes of the cavities, instead of the thermal vacuum. The numerical results show that the cavity-enhanced nonlinear interaction leads to a considerable biphoton generation rate. Using reasonable parameters, such as large pumping detuning and large cavity leaking rate, the purity of the heralded photon should be increased and this is important for the quantum communication and quantum computation. The large pumping detuning allows us to simplify the description of the biphoton generation, and leads to an effective Hamiltonian and reasonable expressions for the biphoton states in the extreme cases with weak and strong cavity leaking.

Filtered by the cavity, only the photons within the range of κ arrive at the detectors. Thus the linewidth of the photon pair can be further reduced if a high-quality cavity is used. The maximal generation rate should be obtained at the double-photon resonance $\omega = 0$, where the anti-Stokes photons are able to transmit out of the system, thanks to the EIT window created by the coupling field. The depth of the EIT (residual absorption) depends on the decoherence rate between the ground levels. Without collisions between atoms and cavity walls, the decoherence rate vanishes. In the realistic setup, the pumping and the coupling lasers have finite linewidths, which leads to the finite decoherence rate and certainly reduces the generation rate due to the absorptions.

APPENDIX: THE EQUATIONS OF THE ELEMENT OF THE DENSITY MATRIX

Based on the master equation (2), the elements of the density matrix obey the following equations:

$$\frac{d}{dt}\rho_{11;m_s n_s;m_{as} n_{as}} = \Gamma_{31}\rho_{33;m_s n_s;m_{as} n_{as}} + \Gamma_{41}\rho_{44;m_s n_s;m_{as} n_{as}} - i\big(g_{as}\sqrt{n_{as}}\rho_{13;m_s n_s;m_{as},n_{as}-1} + \Omega_p\rho_{14;m_s n_s;m_{as} n_{as}}$$
$$- g_{as}\sqrt{m_{as}}\rho_{31;m_s,n_s;m_{as}-1,n_{as}} - \Omega_p^*\rho_{41;m_s n_s;m_{as} n_{as}}\big),$$

$$\frac{d}{dt}\rho_{22;m_s n_s;m_{as} n_{as}} = \Gamma_{32}\rho_{33;m_s n_s;m_{as} n_{as}} + \Gamma_{42}\rho_{44;m_s n_s;m_{as} n_{as}} - i\big(g_s\sqrt{n_s}\rho_{24;m_s,n_s-1;m_{as},n_{as}} + \Omega_c\rho_{23;m_s n_s;m_{as} n_{as}}$$
$$- g_s\sqrt{m_s}\rho_{42;m_s-1,n_s;m_{as},n_{as}} - \Omega_c^*\rho_{32;m_s n_s;m_{as} n_{as}}\big),$$

$$\frac{d}{dt}\rho_{33;m_s n_s;m_{as} n_{as}} = -(\Gamma_{31} + \Gamma_{32})\rho_{33;m_s n_s;m_{as} n_{as}} - i\big(g_{as}\sqrt{n_{as}+1}\rho_{31;m_s,n_s;m_{as},n_{as}+1} + \Omega_c^*\rho_{32;m_s n_s;m_{as} n_{as}}$$
$$- g_{as}\sqrt{m_{as}+1}\rho_{13;m_s n_s;m_{as}+1,n_{as}} - \Omega_c\rho_{23;m_s n_s;m_{as} n_{as}}\big),$$

$$\frac{d}{dt}\rho_{44;m_s n_s;m_{as} n_{as}} = -(\Gamma_{41} + \Gamma_{42})\rho_{44;m_s n_s;m_{as} n_{as}} - i\big(g_s\sqrt{n_s+1}\rho_{42;m_s,n_s+1;m_{as},n_{as}} + \Omega_p^*\rho_{41;m_s n_s;m_{as} n_{as}}$$
$$- g_s\sqrt{m_s+1}\rho_{24;m_s+1,n_s;m_{as},n_{as}} - \Omega_p\rho_{14;m_s n_s;m_{as} n_{as}}\big),$$

$$\frac{d}{dt}\rho_{21;m_s n_s;m_{as} n_{as}} = -(\gamma_{21} + i\omega)\rho_{21;m_s n_s;m_{as} n_{as}} - i\big(g_{as}\sqrt{n_{as}}\rho_{23;m_s,n_s;m_{as},n_{as}-1} + \Omega_p\rho_{24;m_s n_s;m_{as} n_{as}}$$
$$- g_s\sqrt{m_s}\rho_{41;m_s-1,n_s;m_{as},n_{as}} - \Omega_c^*\rho_{31;m_s n_s;m_{as} n_{as}}\big),$$

$$\frac{d}{dt}\rho_{31;m_s n_s;m_{as} n_{as}} = -(\gamma_{31} - i\omega)\rho_{31;m_s n_s;m_{as} n_{as}} - i\big(g_{as}\sqrt{n_{as}}\rho_{33;m_s,n_s;m_{as},n_{as}-1} + \Omega_p\rho_{34;m_s n_s;m_{as} n_{as}}$$
$$- g_{as}\sqrt{m_{as}+1}\rho_{11;m_s n_s;m_{as}+1,n_{as}} - \Omega_c\rho_{21;m_s n_s;m_{as} n_{as}}\big),$$

$$\frac{d}{dt}\rho_{32;m_s n_s;m_{as} n_{as}} = -(\gamma_{32} - 2i\omega)\rho_{32;m_s n_s;m_{as} n_{as}} - i\big(g_s\sqrt{n_s}\rho_{34;m_s,n_s-1;m_{as},n_{as}} + \Omega_c\rho_{33;m_s n_s;m_{as} n_{as}}$$
$$- g_{as}\sqrt{m_{as}+1}\rho_{12;m_s,n_s;m_{as}+1,n_{as}} - \Omega_c\rho_{22;m_s n_s;m_{as} n_{as}}\big),$$

$$\frac{d}{dt}\rho_{43;m_s n_s;m_{as} n_{as}} = -[\gamma_{43} - i(\Delta_p - \omega)]\rho_{43;m_s n_s;m_{as} n_{as}} - i\big(g_{as}\sqrt{n_{as}+1}\rho_{41;m_s,n_s;m_{as},n_{as}+1} + \Omega_c^*\rho_{42;m_s n_s;m_{as} n_{as}}$$
$$- g_s\sqrt{m_s+1}\rho_{23;m_s+1,n_s;m_{as},n_{as}} - \Omega_p\rho_{13;m_s n_s;m_{as} n_{as}}\big),$$

$$\frac{d}{dt}\rho_{41;m_s n_s;m_{as} n_{as}} = -(\gamma_{41} - i\Delta_p)\rho_{41;m_s n_s;m_{as} n_{as}} - i\big(g_{as}\sqrt{n_{as}}\rho_{43;m_s,n_s;m_{as},n_{as}-1} + \Omega_p\rho_{44;m_s n_s;m_{as} n_{as}}$$
$$- g_s\sqrt{m_s+1}\rho_{21;m_s+1,n_s;m_{as},n_{as}} - \Omega_p\rho_{11;m_s n_s;m_{as} n_{as}}\big),$$

$$\frac{d}{dt}\rho_{42;m_s n_s;m_{as} n_{as}} = -[\gamma_{42} - i(\Delta_p + \omega)]\rho_{42;m_s n_s;m_{as} n_{as}} - i\big(g_s\sqrt{n_s}\rho_{44;m_s,n_s-1;m_{as},n_{as}} + \Omega_c\rho_{43;m_s n_s;m_{as} n_{as}}$$
$$- g_s\sqrt{m_s+1}\rho_{22;m_s+1,n_s;m_{as},n_{as}} - \Omega_p\rho_{12;m_s n_s;m_{as} n_{as}}\big).$$

In each equation, there is a hidden term resulting from the $\mathscr{L}_{\mathrm{cav}}(\rho)$, which is

$$\mathscr{D}(\rho_{\alpha\beta;m_s n_s;m_{as} n_{as}}) = -\frac{\kappa_1}{2}(m_s + n_s)\rho_{\alpha\beta;m_s n_s;m_{as} n_{as}} + \kappa_1\sqrt{(m_s+1)(n_s+1)}\rho_{\alpha\beta;m_s+1,n_s+1;m_{as} n_{as}}$$
$$- \frac{\kappa_2}{2}(m_{as} + n_{as})\rho_{\alpha\beta;m_s n_s;m_{as} n_{as}} + \kappa_2\sqrt{(m_{as}+1)(n_{as}+1)}\rho_{\alpha\beta;m_s n_s;m_{as}+1,n_{as}+1}.$$

The atomic decoherence rates γ_{ij} are $\gamma_{31} = \frac{1}{2}(\Gamma_{31} + \Gamma_{32})$, $\gamma_{32} = \frac{1}{2}(\Gamma_{31} + \Gamma_{32})$, $\gamma_{41} = \frac{1}{2}(\Gamma_{41} + \Gamma_{42})$, $\gamma_{42} = \frac{1}{2}(\Gamma_{41} + \Gamma_{42})$, and $\gamma_{43} = \frac{1}{2}(\Gamma_{31} + \Gamma_{32} + \Gamma_{41} + \Gamma_{42})$.

[1] K. Chen, C.-M. Li, Q. Zhang, Y.-A. Chen, A. Goebel, S. Chen, A. Mair, and J.-W. Pan, Experimental realization of one-way quantum computing with two-photon four-qubit cluster states, Phys. Rev. Lett. **99**, 120503 (2007).

[2] W.-B. Gao, P. Xu, X.-C. Yao, O. Gühne, A. Cabello, C.-Y. Lu, C.-Z. Peng, Z.-B. Chen, and J.-W. Pan, Experimental realization of a controlled-not gate with four-photon six-qubit cluster states, Phys. Rev. Lett. **104**, 020501 (2010).

[3] S. E. Harris, M. K. Oshman, and R. L. Byer, Observation of tunable optical parametric fluorescence, Phys. Rev. Lett. **18**, 732 (1967).

[4] S. Massar and S. Clemmen, Resource efficient single photon source based on active frequency multiplexing, Opt. Lett. **46**, 2832 (2021).

[5] A. Agustí, C. W. Sandbo Chang, F. Quijandría, G. Johansson, C. M. Wilson, and C. Sabín, Tripartite genuine non-Gaussian entanglement in three-mode spontaneous parametric down-conversion, Phys. Rev. Lett. **125**, 020502 (2020).

[6] S. Du, J. Wen, and M. H. Rubin, Narrowband biphoton generation near atomic resonance, J. Opt. Soc. Am. B **25**, C98 (2008).

[7] L. Zhao, X. Guo, Y. Sun, Y. Su, M. M. T. Loy, and S. Du, Shaping the biphoton temporal waveform with spatial light modulation, Phys. Rev. Lett. **115**, 193601 (2015).

[8] L. Zhao, X. Guo, C. Liu, Y. Sun, M. M. T. Loy, and S. Du, Photon pairs with coherence time exceeding 1 μs, Optica **1**, 84 (2014).

[9] S. Du, P. Kolchin, C. Belthangady, G. Y. Yin, and S. E. Harris, Subnatural linewidth biphotons with controllable temporal length, Phys. Rev. Lett. **100**, 183603 (2008).

[10] Y.-S. Wang, K.-B. Li, C.-F. Chang, T.-W. Lin, J.-Q. Li, S.-S. Hsiao, J.-M. Chen, Y.-H. Lai, Y.-C. Chen, Y.-F. Chen, C.-S. Chuu, and I. A. Yu, Temporally ultralong biphotons with a linewidth of 50 kHz, APL Photon. **7**, 126102 (2022).

[11] M. Fleischhauer, A. Imamoglu, and J. P. Marangos, Electromagnetically induced transparency: Optics in coherent media, Rev. Mod. Phys. **77**, 633 (2005).

[12] M. Förtsch, J. U. Fuerst, C. Wittmann, D. Strekalov, A. Aiello, M. V. Chekhova, C. Silberhorn, G. Leuchs, and C. Marquardt, A versatile source of single photons for quantum information processing, Nat. Commun. **4**, 1818 (2013).

[13] H. J. Kimble, The quantum internet, Nature (London) **453**, 1023 (2008).

[14] Y.-F. Hsiao, P.-J. Tsai, H.-S. Chen, S.-X. Lin, C.-C. Hung, C.-H. Lee, Y.-H. Chen, Y.-F. Chen, I. A. Yu, and Y.-C. Chen, Highly efficient coherent optical memory based on electromagnetically induced transparency, Phys. Rev. Lett. **120**, 183602 (2018).

[15] Y. Wang, J. Li, S. Zhang, K. Su, Y. Zhou, K. Liao, S. Du, H. Yan, and S.-L. Zhu, Efficient quantum memory for single-photon polarization qubits, Nat. Photon. **13**, 346 (2019).

[16] P.-J. Tsai, Y.-F. Hsiao, and Y.-C. Chen, Quantum storage and manipulation of heralded single photons in atomic memories based on electromagnetically induced transparency, Phys. Rev. Res. **2**, 033155 (2020).

[17] D. Tiarks, S. Schmidt-Eberle, T. Stolz, G. Rempe, and S. Duerr, A photon-photon quantum gate based on Rydberg interactions, Nat. Phys. **15**, 124 (2019).

[18] J. Vaneecloo, S. Garcia, and A. Ourjoumtsev, Intracavity Rydberg superatom for optical quantum engineering: Coherent control, single-shot detection, and optical π phase shift, Phys. Rev. X **12**, 021034 (2022).

[19] T. Stolz, H. Hegels, M. Winter, B. Röhr, Y.-F. Hsiao, L. Husel, G. Rempe, and S. Dürr, Quantum-logic gate between two optical photons with an average efficiency above 40%, Phys. Rev. X **12**, 021035 (2022).

[20] S. Du, Quantum-state purity of heralded single photons produced from frequency-anticorrelated biphotons, Phys. Rev. A **92**, 043836 (2015).

[21] P. J. Mosley, J. S. Lundeen, B. J. Smith, P. Wasylczyk, A. B. U'Ren, C. Silberhorn, and I. A. Walmsley, Heralded generation of ultrafast single photons in pure quantum states, Phys. Rev. Lett. **100**, 133601 (2008).

[22] M. Rambach, A. Nikolova, T. J. Weinhold, and A. G. White, Sub-megahertz linewidth single photon source, APL Photon. **1**, 096101 (2016).

[23] J. Liu, J. Liu, P. Yu, and G. Zhang, Sub-megahertz narrow-band photon pairs at 606 nm for solid-state quantum memories, APL Photon. **5**, 066105 (2020).

[24] The cavity-enhanced biphoton generation based on the non-linear process ($2\omega_{\text{pump}} \rightarrow \omega_{\text{signal}} + \omega_{\text{idler}}$) which is very similar to the SPDC process is well studied, see, e.g. E. A. Goldschmidt, M. D. Eisaman, J. Fan, S. V. Polyakov, and A. Migdall, Spectrally bright and broad fiber-based heralded single-photon source, Phys. Rev. A **78**, 013844 (2008); M. Kamandar Dezfouli, M. M. Dignam, M. J. Steel, and J. E. Sipe, Heisenberg treatment of pair generation in lossy coupled-cavity systems, ibid. **90**, 043832 (2014); M. A. Seidler, X. J. Yeo, A. Cerè, and C. Kurtsiefer, Spectral compression of narrowband single photons with a resonant cavity, Phys. Rev. Lett. **125**, 183603 (2020); T. J. Steiner, J. E. Castro, L. Chang, Q. Dang, W. Xie, J. Norman, J. E. Bowers, and G. Moody, Ultrabright entangled-photon-pair generation from an AlGaAs-on-insulator microring resonator, PRX Quantum **2**, 010337 (2021).

[25] N. Gisin, G. Ribordy, W. Tittel, and H. Zbinden, Quantum cryptography, Rev. Mod. Phys. **74**, 145 (2002).

[26] A. Seri, D. Lago-Rivera, A. Lenhard, G. Corrielli, R. Osellame, M. Mazzera, and H. de Riedmatten, Quantum storage of frequency-multiplexed heralded single photons, Phys. Rev. Lett. **123**, 080502 (2019).

[27] J. Lugani, R. J. A. Francis-Jones, J. Boutari, and I. A. Walmsley, Spectrally pure single photons at telecommunications wavelengths using commercial birefringent optical fiber, Opt. Express **28**, 5147 (2020).

[28] S. L. Braunstein and P. van Loock, Quantum information with continuous variables, Rev. Mod. Phys. **77**, 513 (2005).

[29] V. Giovannetti, S. Lloyd, and L. Maccone, Quantum metrology, Phys. Rev. Lett. **96**, 010401 (2006).

[30] S. Lloyd, Universal quantum simulators, Science **273**, 1073 (1996).

[31] Z.-Y. Shi, H. Tang, Z. Feng, Y. Wang, Z.-M. Li, J. Gao, Y.-J. Chang, T.-Y. Wang, J.-P. Dou, Z.-Y. Zhang, Z.-Q. Jiao, W.-H. Zhou, and X.-M. Jin, Quantum fast hitting on glued trees mapped on a photonic chip, Optica **7**, 613 (2020).

[32] R. Loudon, *The Quantum Theory of Light*, 3rd ed. (Oxford University Press, New York, 2000).

[33] T.-J. Shih, W.-K. Huang, Y.-M. Lin, K.-B. Li, C.-Y. Hsu, J.-M. Chen, P.-Y. Tu, T. Peters, Y.-F. Chen, and I. A. Yu, Universal relation between the conditional auto-correlation function and the cross-correlation function of biphotons, Opt. Express **32**, 13657 (2024).

[34] G. Brassard, N. Lütkenhaus, T. Mor, and B. C. Sanders, Limitations on practical quantum cryptography, Phys. Rev. Lett. **85**, 1330 (2000).

[35] P. Senellart, G. Solomon, and A. White, High-performance semiconductor quantum-dot single-photon sources, Nat. Nanotechnol. **12**, 1026 (2017).

[36] N. Spagnolo, C. Vitelli, M. Bentivegna, D. J. Brod, A. Crespi, F. Flamini, S. Giacomini, G. Milani, R. Ramponi, P. Mataloni, R. Osellame, E. F. Galvao, and F. Sciarrino, Experimental validation of photonic boson sampling, Nat. Photon. **8**, 615 (2014).

[37] M. A. Broome, A. Fedrizzi, S. Rahimi-Keshari, J. Dove, S. Aaronson, T. C. Ralph, and A. G. White, Photonic boson sampling in a tunable circuit, Science **339**, 794 (2013).

[38] L. Zhao, Y. Su, and S. Du, Narrowband biphoton generation in the group delay regime, Phys. Rev. A **93**, 033815 (2016).

[39] E. Will, L. Masters, A. Rauschenbeutel, M. Scheucher, and J. Volz, Coupling a single trapped atom to a whispering-gallery-mode microresonator, Phys. Rev. Lett. **126**, 233602 (2021).

[40] B. Weber, H. P. Specht, T. Müller, J. Bochmann, M. Mücke, D. L. Moehring, and G. Rempe, Photon-photon entanglement with a single trapped atom, Phys. Rev. Lett. **102**, 030501 (2009).

[41] K. M. Fortier, S. Y. Kim, M. J. Gibbons, P. Ahmadi, and M. S. Chapman, Deterministic loading of individual atoms to a high-finesse optical cavity, Phys. Rev. Lett. **98**, 233601 (2007).

[42] P. Maunz, T. Puppe, I. Schuster, N. Syassen, P. W. H. Pinkse, and G. Rempe, Normal-mode spectroscopy of a single-bound-atom–cavity system, Phys. Rev. Lett. **94**, 033002 (2005).

[43] P. Kolchin, S. Du, C. Belthangady, G. Y. Yin, and S. E. Harris, Generation of narrow-bandwidth paired photons: Use of a single driving laser, Phys. Rev. Lett. **97**, 113602 (2006).

[44] Vlatko Balić, D. A. Braje, P. Kolchin, G. Y. Yin, and S. E. Harris, Generation of paired photons with controllable waveforms, Phys. Rev. Lett. **94**, 183601 (2005).

[45] P. Kolchin, Electromagnetically-induced-transparency-based paired photon generation, Phys. Rev. A **75**, 033814 (2007).

[46] P. M. Alsing and E. E. Hach, Photon-pair generation in a lossy microring resonator. I. Theory, Phys. Rev. A **96**, 033847 (2017).

[47] D. N. Klyshko, *Photons and Nonlinear Optics* (Gordon and Breach Science, New York, 1988).

[48] The damping processes are modeled as the interaction between the main system and a group of the harmonic oscillators as a reservoir. See,e.g., M. O. Scully and M. S. Zubairy, *Quantum Optics* (Cambridge University Press, Cambridge, 1997).

[49] C. Cohen-Tannoudji, J. Dupont-Roc, and G. Grynberg, *Atom-Photon Interactions* (Wiley, Weinheim, Germany, 1998).

[50] R. Kosloff, Quantum thermodynamics: A dynamical viewpoint, Entropy **15**, 2100 (2013).

[51] P. P. Hofer, M. Perarnau-Llobet, L. D. M. Miranda, G. Haack, R. Silva, J. B. Brask, and N. Brunner, Markovian master equations for quantum thermal machines: Local versus global approach, New J. Phys. **19**, 123037 (2017).

[52] M. Cattaneo, G. L. Giorgi, S. Maniscalco, and R. Zambrini, Local versus global master equation with common and separate baths: Superiority of the global approach in partial secular approximation, New J. Phys. **21**, 113045 (2019).

[53] J.-M. Chen, C.-Y. Hsu, W.-K. Huang, S.-S. Hsiao, F.-C. Huang, Y.-H. Chen, C.-S. Chuu, Y.-C. Chen, Y.-F. Chen, and I. A. Yu, Room-temperature biphoton source with a spectral brightness near the ultimate limit, Phys. Rev. Res. **4**, 023132 (2022).

[54] X. Guo, Y. Mei, and S. Du, Single photon at a configurable quantum-memory-based beam splitter, Phys. Rev. A **97**, 063805 (2018).

[55] B. Srivathsan, G. K. Gulati, B. Chng, G. Maslennikov, D. Matsukevich, and C. Kurtsiefer, Narrow band source of transform-limited photon pairs via four-wave mixing in a cold atomic ensemble, Phys. Rev. Lett. **111**, 123602 (2013).

[56] R. Hanbury Brown and R. Q. Twiss, Correlation between photons in two coherent beams of light, Nature (London) **177**, 27 (1956).

[57] M. D. Reid and D. F. Walls, Violations of classical inequalities in quantum optics, Phys. Rev. A **34**, 1260 (1986).